Polym. Korea, Vol. 49, No. 5, pp. 536-547 (2025)
https://doi.org/10.7317/pk.2025.49.5.536
ISSN 2234-8077(Online)

MXenes/에폭시 복합재의 제조 및 경화 동역학 연구

Wei Xu†

Military Industry Project Audit Center, State Administration of Science, Technology and Industry for National Defence

(2024년 12월 10일 접수, 2025년 4월 10일 수정, 2025년 4월 15일 채택)

Preparation of MXenes/epoxy Composites and Curing Kinetics Study

Wei Xu†

Military Industry Project Audit Center, State Administration of Science, Technology and Industry for National Defence, PRC, Beijing 100037, China

(Received December 10, 2024; Revised April 10, 2025; Accepted April 15, 2025)

Abstract: In this study, using selective etching method, MXenes ($Ti_3C_2T_x$) were prepared and were carefully characterized by wide-angle X-ray diffraction, scanning electron microscopy and transmission electron microscopy. Obtained results revealed the successful preparation of MXenes. After that, epoxy resin (EP)/MXenes composites containing 0.25-1 wt% MXenes were prepared. Morphology study of the fractured surface of the samples revealed that the MXenes are finely dispersed in the EP matrix; Curing kinetics study revealed that the addition of MXenes can effectively reduce the curing characteristic temperatures of EP, promoting the curing process to proceed at lower temperatures. Among them, the curing temperatures and curing rate of EP/MX1 with the addition of 1 wt% MXenes are highest and reaches the peak curing rate. Moreover, the EP/MX1 exhibits the highest curing degree; Using Kissinger method, we found that MXenes significantly reduced the reaction activation energy (E_a) of EP. Within the scope of this study, the amount of MXenes added is directly proportional to the degree of reduction in E_a. Compared to pure EP, 52687 J/mol decreased to 40503 J/mol, a decrease of 23.8%; The Ozawa method calculation results show that under the same degree of conversion, the apparent E_a of EP/MX1 is the lowest. The influence of MXenes on the curing behavior of EP was discussed, related mechanism was proposed. Moreover, results of dynamic mechanical analysis (DMA) revealed that the glass transition temperature increases gradually with the increase of the MXenes content, indicating that the presence of MXenes promotes the crosslinking of EP.

Keywords: MXenes, polymer composites, epoxy, curing kinetics.

Introduction

Epoxy resin (EP), as a thermosetting resin with high performance, has excellent heat resistance, chemical stability, electrical performance, adhesion and processing performance, which is widely applied in adhesives, coatings, engineering materials.[1,2] High cross-linking density can bring advantages such as high modulus and excellent thermal performance to epoxy resin.[2] However, after curing process, the linear molecules formed cross-linking network structure, which limits the movement of molecular chains, resulting in the disadvantages such as high brittleness and poor fracture toughness,[3,4] and limited dielectric properties, which greatly limits its development in some fields.[5]

By doping nanoparticles to prepare EP composites with high-performance, EP is optimized in terms of mechanical and dielectric properties,[6,7] and endowed with new properties such as high thermal conductivity, high conductivity, and electromagnetic shielding performance,[8] further meeting the strict requirements of various fields of application.[9,10]

Nanoparticles usually have large specific surface area, excellent toughness and strength, as well as high conductivity and thermal conductivity.[11-13] Due to their large specific surface area, their surface functional groups can react with EP to form a cross-linked network, thereby improving the performance of composite materials.[14-16] Nanoparticles mainly include inorganic nanometallic oxides,[17,18] carbon based nanoparticles,[19-22] etc. The impacts of nanoparticles on EP are quite complex, *i.e.*, the concentration, type, morphology, and size of the nanocomposites all have impacts on the performance of composite materials.[23,24] Many researchers have conducted extensive research

†To whom correspondence should be addressed.
xwsastind@163.com, ORCID 0009-0000-2437-4347

on this topic.[25]

Inorganic nano metal oxides mainly include TiO_2, Al_2O_3, MXenes, etc. Bazrgari *et al*.[26] used ultrasonic stirring to uniformly disperse Al_2O_3 into EP, and improved the bending strength and impact strength of the EP. In addition, adding Al_2O_3 nanoparticles at lower concentrations significantly reduced the wear rate and friction coefficient of the epoxy resin matrix.

Zhang *et al*.[27] doped EP with a hybrid filler composed of modified Al_2O_3 and modified sulfite (ATP) inorganic materials, enhancing the mechanical, dynamic mechanical, and dielectric properties of EP composite materials. Zhao *et al*.[28] successfully prepared *n*-octadecane@TiO_2 particles in oil in water solution by sol-gel method, and added the obtained core-shell particles into EP to prepare EP composites. Compared with pure EP and TiO_2 doped EP, its wear rate and friction coefficient decreased. Dong *et al*.[29] reviewed the properties of several 2D materials and the methods of compositing 2D materials with EP, mainly focusing on the regulation methods to improve the dispersion of 2D materials in epoxy resins and the interfacial interaction of 2D materials with epoxy resins; Han *et al*.[30] comparatively studied the effect of two types of 2D nanofillers, boron nitride sheets and graphene platelets, on the mechanical properties and thermal conductivity of epoxy resin. They emphasized the importance of adding low dosage of thin nanosheets (thickness 3–5 nm) to prepare EP composites with desired mechanical and thermal properties.

MXenes, being a 2D inorganic metal oxide, are composed of transition metal carbides, nitrides, or carbonitrides in the size of several atomic layer thicknesses.[18] MXenes are obtained by MAX phase treatment,[31] and the specific molecular formula of MAX phase is $M_{n+1}AX_n$ (n = 1, 2 or 3), where M represents the transition metals of the previous groups, A corresponds the main group elements, while X is the C and/or N elements. There exists strong bonding energy between M and X, while A has active chemical activity, therefore, A can be removed from the MAX phase through etching, resulting in the 2D structure of MXenes.[32]

MXenes have the mixed properties of metal/covalent/ion in M-X bonds, and introduce surface functional groups (-F, -O, -OH) through acid etching.[29] They have outstanding advantages such as good conductivity, outstanding mechanical properties, adjustable bandgap, high volume capacitance, strong hydrophilicity, and high thermal conductivity.[18,33] Therefore, they can be applied in many fields such as energy storage, microwave absorption, catalysts, sensors, and biomedicine.[18,29,31,34,35]

Sliozberg *et al*.[29] used theoretical simulations to study the binding energy and micro fracture mechanism of EP/MXenes composites under uniaxial tension. Then, they prepared EP/MXenes composites and studied their structure and fracture surface, verifying the correctness of the simulation results.

Chen *et al*.[18] performed ion intercalation and ultrasound assistance, followed by thermal reduction at medium and low temperatures to prepare MXenes, and then prepared EP/MXenes composites for electromagnetic interference shielding using solution casting method; Cabanelas *et al*.[32] summarized the latest development progress of EP/MXenes composites and the contribution of MXenes nanofillers to the enhancement performance of EP, particularly discussing their applications in protective coatings, electromagnetic interference shielding, and composite materials. Finally, the remaining challenges in this field were discussed; Wu *et al*.[33] reported a simple method for synthesizing $Ti_3C_2T_x$ MXenes nanosheets and the preparation method for a novel conductive adhesive based on EP matrix; Zhou *et al*.[30] used acid-etching method to prepare $Ti_3C_2T_x$ and bimetallic MXenes ($Mo_2Ti_2C_3T_x$) and then introduced them into EP for the comparative investigation of their flame-retardant effect. The results revealed that MXenes were finely dispersed in EP matrix, which can contribute to the improvements of thermal and flame retardant properties of EP composites.

In summary, EP/MXenes composites can endow EP with excellent comprehensive properties, which have been studied by some scholars. However, the performance of EP composites depends not only on the structure and performance of EP, curing agents, and additives, but also on its molding and curing process. The structure and properties of cured products obtained from the same formula under different curing process parameters and procedures have significant differences, so the study of curing kinetics is crucial. However, there is currently little research on the impact of curing kinetics on EP/MXenes composite materials, and no one has reported the mechanism of action of MXenes at different concentrations on EP curing kinetics. This study firstly prepared MXenes and characterized its microstructure. Then, a series of EP/MXenes composite materials were prepared, and their curing kinetics were thoroughly studied. The mechanisms of MXenes and its concentrations on the curing behavior and curing kinetics of EP/MXenes composites were explored.

Experimental

Materials and Sample Preparation. Materials: Epoxy resin (EP), Bisphenol A type, tradename E51, was provided by Deyuan Chemical Corp., Beijing, China; Amine curing agent JH-0422,

was provided by Changshu Jiafa Chemical Corp. Beijing, China; The Ti_3AlC_2 MAX-phase powder (99% purity), was provided by 11 Technology Co. Ltd. (Beijing, China); Lithium fluoride (LiF, 99% purity) was provided by Aladdin Bio-Chem Technology Co. Ltd. (Shanghai, China); Concentrated hydrochloric acid (HCl, 37 wt%) was provided by Chengdu Kelong Chemical Reagent Factory (Chengdu, China).

Preparation of MXenes ($Ti_3C_2T_x$): This work used HCl and LiF to form HF and selectively etch Ti_3AlC_2, based on previous studies.[18,29-31] Firstly, LiF was dissolved in dilute HCl (6M) under magnetic stirring for 10 min. Then, Ti_3AlC_2 powder was slowly added within 10 min to avoid any possible overheating caused by the reaction. Then, the solution was heated under magnetic stirring at 40 ℃ for 24 hours. When the etching was completed, solution was centrifuged at 8000 rpm for 10 min, and then it was washed with distilled water. The washing process was repeated to remove residual reaction products until the pH of the supernatant was approximately 7. Then distilled water was added to the sediment and it was placed in ice water bath, followed by 2 h of ultrasonic treatment and centrifugation. Finally, the obtained suspension was dried under vacuum.

Preparation of EP/MXenes Composites: Firstly, certain amount of MXenes was added to 500 mL of ethanol in a beaker and sonicated for 2 h to obtain MXenes dispersion. Subsequently, 5 g EP was added into MXenes dispersion and sonicated for 2 h at 25 ℃. Then, the solution was heated with 90 ℃ oil bath and stirred for 12 h to evaporate ethanol. After that, it was vacuum dried for 2 h in 90 ℃ vacuum oven to remove residual ethanol.[36] Finally, the curing agent (20 wt% of the epoxy prepolymer) was added and stirred until a uniform EP/MXenes composites were obtained. Using this method, pure EP and EP/MXenes composite materials were prepared. The concentrations of MXenes are 0.25, 0.5, 0.75, and 1 wt%, and the resulting composites are named as EP/MX0.25, EP/MX0.5, EP/MX0.75, and EP/MX1, respectively.

Characterizations. Wide-angle X-ray Diffraction (WAXD): The WAXD patterns of MXenes were measured using Ultima IV diffractor (Rigaku Co., Japan). The radiation CuK_α, the wavelength $\lambda = 0.154$ nm, the scanning range 2θ was 5-60° and the scanning rate was 2°/min.

Scanning Electron Microscopy (SEM): Morphologies of MXenes were observed using SEM (Nova Nano SEM 450, USA), and the accelerating voltage was 3 kV.[37,38]

Transmission Electron Microscopy (TEM): TEM observation was performed on MXenes by Tecnai G2 F20 (FEI, Hillsborough, Oregon, USA). The sample was firstly dispersed in ethanol and then deposited on a copper grid. Measurement was performed under the accelerating voltage of 200 kV.[39-41]

Differential Scanning Calorimetry (DSC): DSC was performed by METTLER TOLEDO DSC3+ (Mettler Toledo Corp., Zurich, Switzerland). The DSC equipment was firstly calibrated with indium and zinc standards.[42,43] The samples (about 3 mg) were added to aluminum pans, and the curing kinetics measurement was performed in N_2 atmosphere with the heating rates of 5 ℃/min, 10 ℃/min, 15 ℃/min and 20 ℃/min, from room temperature to 300 ℃.[44,45]

Dynamic Mechanical Analysis (DMA): The dynamic mechanical properties of the samples were tested using DMA Q800 (TA Instruments, USA) in a single cantilever beam mode. The testing frequency was 1 Hz, the heating rate was 3 ℃/min, the testing temperature was 0-120 ℃, the applied amplitude was 10 μm, and the sample size was $20 \times 10 \times 4$ mm^3.

Results and Discussions

Characterization of MXenes. WAXD Measurement: WAXD was conducted to elucidate the structure and morphology of the $Ti_3C_2T_x$ powder, as shown in Figure 1. After etching, the sharp (002) diffraction peak of the filler changes from 2θ = 9.6° to 2θ = 6.4°, indicating a significant increase in interlayer distance. Moreover, the peak at 2θ = 38.9° refers to strongest (104) peak of Ti_3AlC_2 also disappears, which indicates that the Al layer has been removed, resulting in a transition from Ti_3AlC_2 to $Ti_3C_2T_x$.

SEM Observation: The morphology of Ti_3AlC_2 and $Ti_3C_2T_x$ was investigated using SEM as shown in Figure 2. Ti_3AlC_2 exhibits a tightly stacked dense layered structure, which is often seen in ternary carbides. After etching process, the thin layers

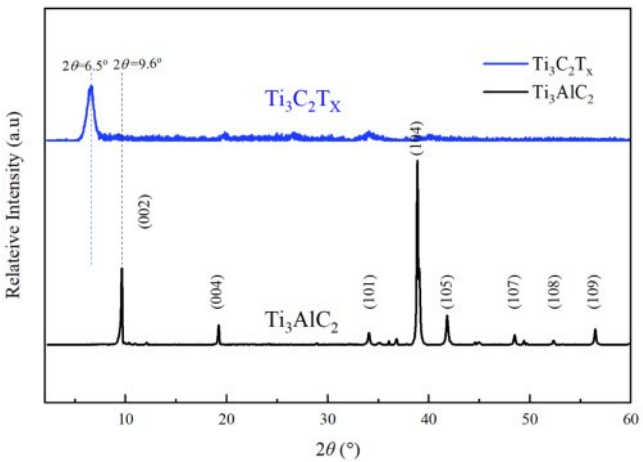

Figure 1. WAXD results of Ti_3AlC_2 and $Ti_3C_2T_x$.

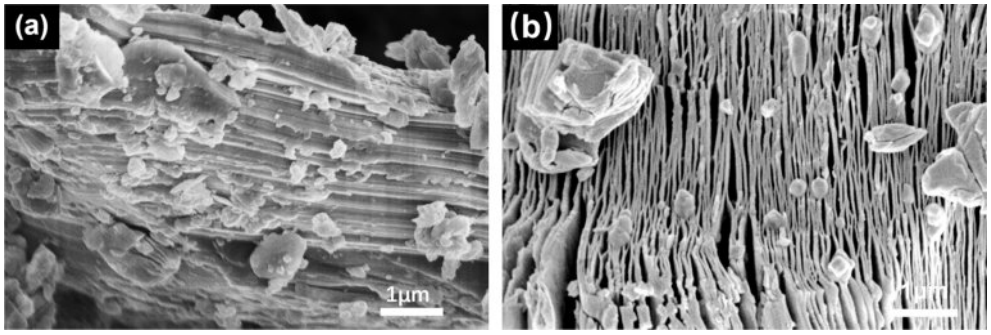

Figure 2. SEM images of (a) Ti_3AlC_2; (b) $Ti_3C_2T_x$.

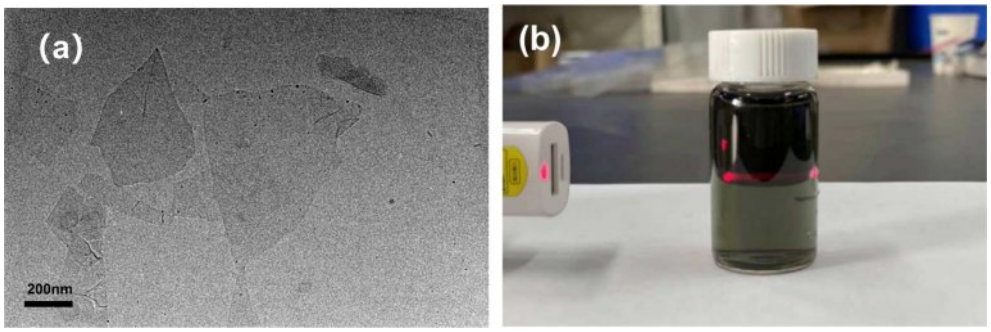

Figure 3. (a) TEM image of $Ti_3C_2T_x$ dispersed in distilled water; (b) digital photos of $Ti_3C_2T_x$ dispersion.

of $Ti_3C_2T_x$ are weakly stacked, and the interlayer distance increases, revealing accordion like morphology, which is in accord with the results of WAXD, which might be due to the exothermic reaction between HF and Al, resulting in the escape of gases such as H_2 during the etching process.

TEM Observation: In order to further investigate the dispersibility of $Ti_3C_2T_x$, it was dispersed in distilled water and then subjected to TEM test. The results obtained are shown in Figure 3(a). $Ti_3C_2T_x$ has a single sheet structure in distilled water, with a transverse size of about a few hundred nanometers in a thin sheet structure. Figure 3b shows a photo of $Ti_3C_2T_x$ dispersed in distilled water. The diluted $Ti_3C_2T_x$ dispersion appears light green and exhibits the Tyndall effect,[46,47] proving that it is nano dispersed in distilled water.

Curing Behavior Investigation. To elucidate the influence of MXenes on the curing behavior of EP, we prepared EP/MXenes composites. The addition amounts of MXenes are respectively 0.25, 0.5, 0.75 and 1 wt%. For the convenience of discussion, the above samples are named MX0.25, MX0.5, MX0.75, and MX1 respectively.

In order to obtain the dispersion of MXenes in EP matrix, the samples were soaked in liquid nitrogen for sufficient time, then, they were used to obtain the fracture surface for SEM observation. The SEM results obtained are shown in Figure 4.

From Figure 4(a), it can be seen that the cross-section of pure EP is relatively flat. After adding 0.25 wt% MXenes, a few short cracks with a length of approximately 1-8 μm appeared on the cross-section of EP/MX0.25 in Figure 4(b), which might be evidence of MXene finely distributed in EP; For EP/MX0.5 in Figure 4(c), due to the increase in MXenes content, it can be seen that the number of cracks increases (as shown by the dotted circle in the figure), and their dispersion is relatively uniform, reflecting the good dispersion of MXenes in EP matrix. Interestingly, these cracks are connected to relatively long strip structures arranged parallel to each other. This might be cracks in the EP matrix caused by stress during fracturing; With the further increase of MXenes content (Figure 4(d)), the cross-section of EP becomes no longer flat, which might indicate that the addition of 0.75 wt% and more MXenes changed the fractured surface morphology of EP. The uniformity of the fractured morphology of EP is good, reflecting the good dispersion of MXene. The possible locations of MXene are also marked with dashed circles. It can be seen that the distribution of MXenes is relatively uniform. For EP/MX1 (Figure 4(e)), the cracks and grooves become smaller and have better uniformity. This might be due to the addition of higher content MXenes, which change the stress distribution and transmission during EP fracturing, leading to an increase in the regions involved in deformation

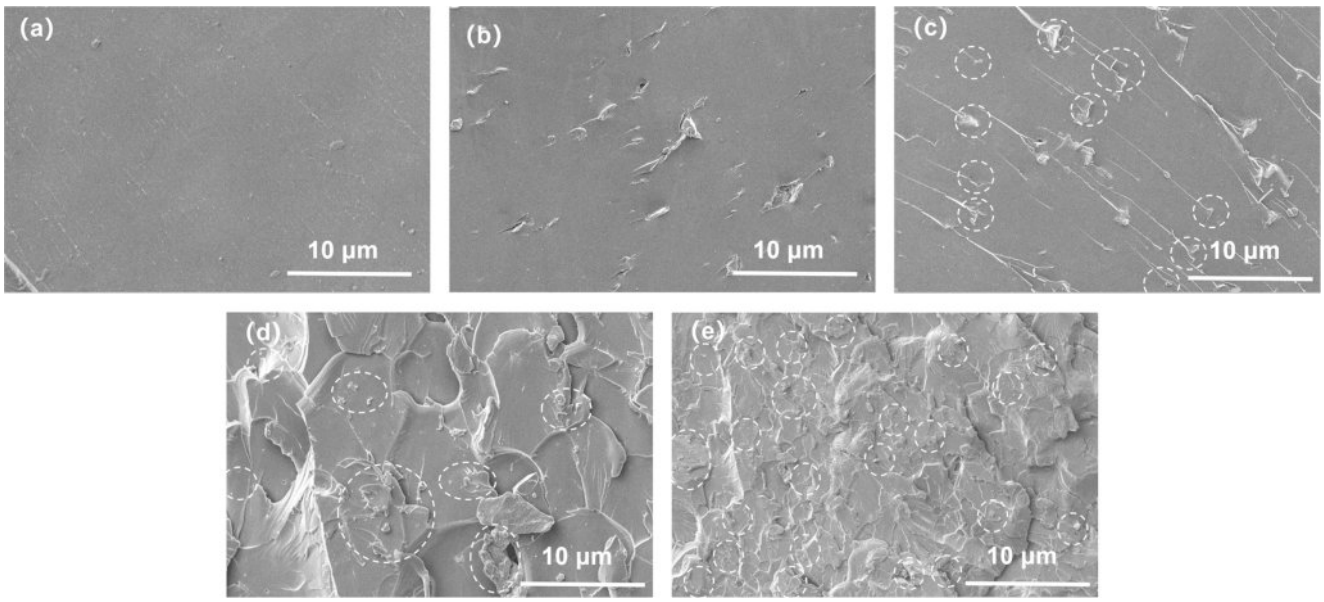

Figure 4. SEM images of the fractured surface of (a) pure EP; (b) EP/MX0.25; (c) EP/MX0.5; (d) EP/MX0.75; (e) EP/MX1.

and energy transmission. The possible locations of MXenes are also marked with dashed circles. Based on these positions and the uniformity of the cross-sectional morphology, it can be concluded that the dispersion of MXenes is good.

The DSC study was used to investigate the curing behavior of neat EP and EP/MXenes composites. Figure 5 shows DSC curves of EP and EP/MXenes composites at heating rates of 5-20 ℃/min. From this, the curing initial temperature (T_i), peak temperature of curing (T_p) and end temperature of curing (T_e) of EP and EP/MXenes composites at different heating rates can also be obtained.

From Figure 5, it can be seen that for each sample, the total enthalpy gradually increases in the early stages of the curing reaction and gradually decreases after reaching the peak temperature. At the same time, after the addition of MXenes, the curing characteristic temperatures (initial curing temperature T_i, curing peak temperature T_p, curing termination temperature T_e) of EP significantly decreased, and the higher the concentration of MXenes added, the more significant the decrease in the above parameters. The reason may be that the surface of MXenes is rich in different types of functional groups, including hydroxyl groups, amino groups, etc., which have similar catalytic effects to -OH formed during the EP curing process. They may react with other functional groups such as C-O-C to generate self-catalysis, which is conducive to the curing chemical reaction between amine curing agents and EP.

The characteristic temperature fitting results obtained from the DSC curves are shown in Figure 6. The results in Figure 6 indicate that there are also differences in the characteristic temperatures of EP/MXenes composites at different heating rates (β). The T-β extrapolation method for curing EP/MXenes composites is a differential scanning calorimetry test conducted on EP/MXenes composites at different heating rates. By analyzing the relationship between the peak temperature of the curing reaction and the heating rate, the theoretical curing reaction temperature at infinite slow heating is extrapolated to determine the optimal curing temperature. This provides an important basis for the formulation of EP/MXenes composites curing processes, research on curing kinetics, and evaluation of curing degree. Adopting T-β extrapolation method, we can obtain the characteristic temperatures when the heating rate (β) approaches 0 ℃/min based on the intercept of the fitted curve, and then roughly determine the curing process parameters of various EP/MXenes composites. The obtained characteristic temperatures include the initial curing temperature (T_i), curing peak temperature (T_p), and curing end temperature (T_e) and total enthalpy are shown in Table 1. From Table 1, after adding MXenes, the various characteristic temperature values of EP/MXenes composites will decrease, and the higher the concentration of MXenes added, the greater the decrease in the above characteristic temperature values. Moreover, the total enthalpy gradually increases with the increase of MXene content, indicating that the presence of MXene makes more fractions of EP takes part in the curing process. This is consistent with the results in Figure 5.

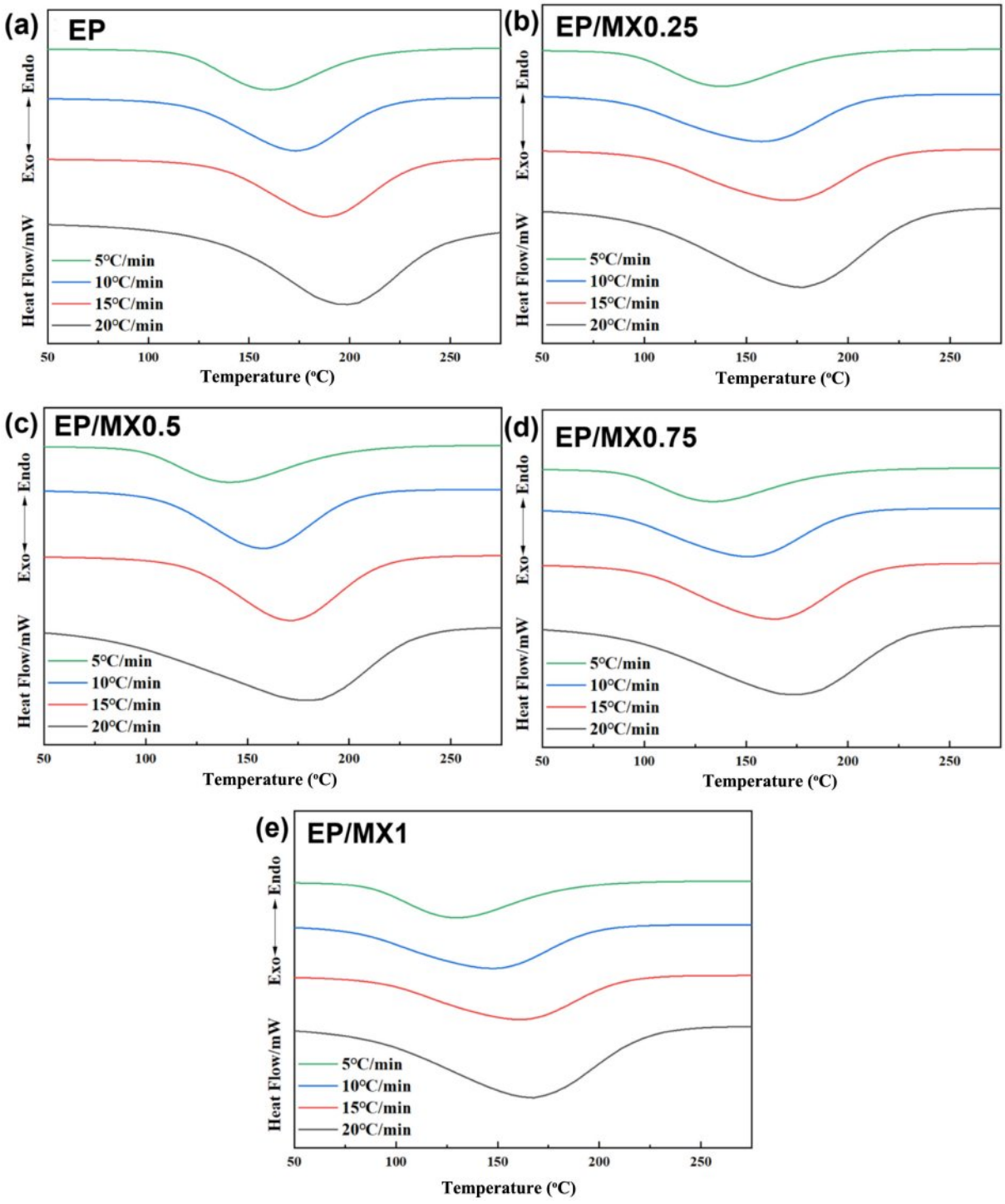

Figure 5. DSC heating curves of (a) EP; (b) EP/MX0.25; (c) EP/MX0.5; (d) EP/MX0.75; (e) EP/MX1 at different heating rates.

Curing Conversion Degree and Curing Rate Study. Figure 7(a) shows conversion degree (reaction degree, α) of EP and EP/MXenes composites at 5 ℃/min heating rate. The result shows that the conversion degree α of all the samples exhibits a typical *S*-shaped curve with the increase of curing temperature, indicating that the EP system has self-catalytic characteristic,[23] and the addition of MXenes does not completely change the mechanism of EP curing reaction; At the same curing temperature, the higher the concentration of MXenes, the higher the degree of curing. The addition of high content

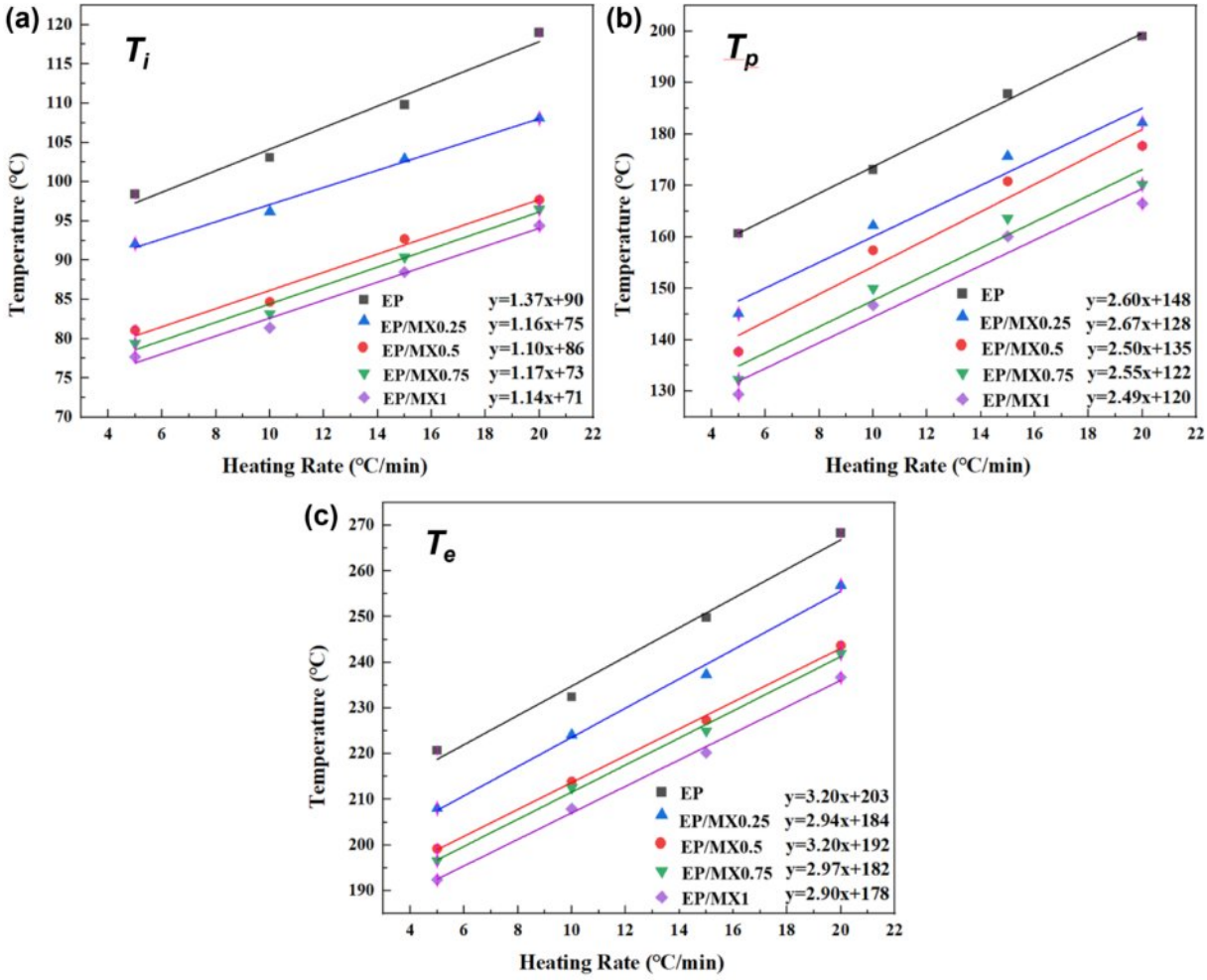

Figure 6. Temperature versus the heating rate β curves of EP, EP/MX0.25, EP/MX0.5, EP/MX0.75 and EP/MX1.

Table 1. T_i, T_p, T_e and Total Enthalpy Values for EP, EP/MX0.25, EP/MX0.5, EP/MX0.75 and EP/MX1 Obtained by Calculating the Intercept Through T-β Extrapolation

Sample Name	EP	EP/MX0.25	EP/MX0.5	EP/MX0.75	EP/MX1
T_i (℃)	90	86	75	73	71
T_p (℃)	148	135	128	122	120
T_e (℃)	203	192	184	182	178
Total enthalpy (J/g)	86.3	93.4	99.1	101.4	102.6

MXenes further promoted the curing process of EP within the scope of this study.

In order to further explore the relationship between the curing rate and curing temperature of the above samples, mathematical differentiation was performed on the curve in Figure 7(a) to obtain the *T*-$d\alpha/dT$ of the samples, as shown in Figure 7(b).

From Figure 7(b), it can be seen that for all samples, the curing rate shows an increasing trend as the temperature increases during the initial curing stage. In this stage, EP/MX1 exhibits the highest curing speed, which reaches peak curing rate at the earliest. This is because the MXenes concentration of EP/MX1 is the highest, and it can be well dispersed in the EP matrix, thus participating more fully in the curing process of EP, forming a stronger cross-linking network structure, and can end the curing reaction faster. For other samples with low MXenes addition, the curing rate actually decreases, and the temperature at which the curing rate peak is reached is also more delayed. At later

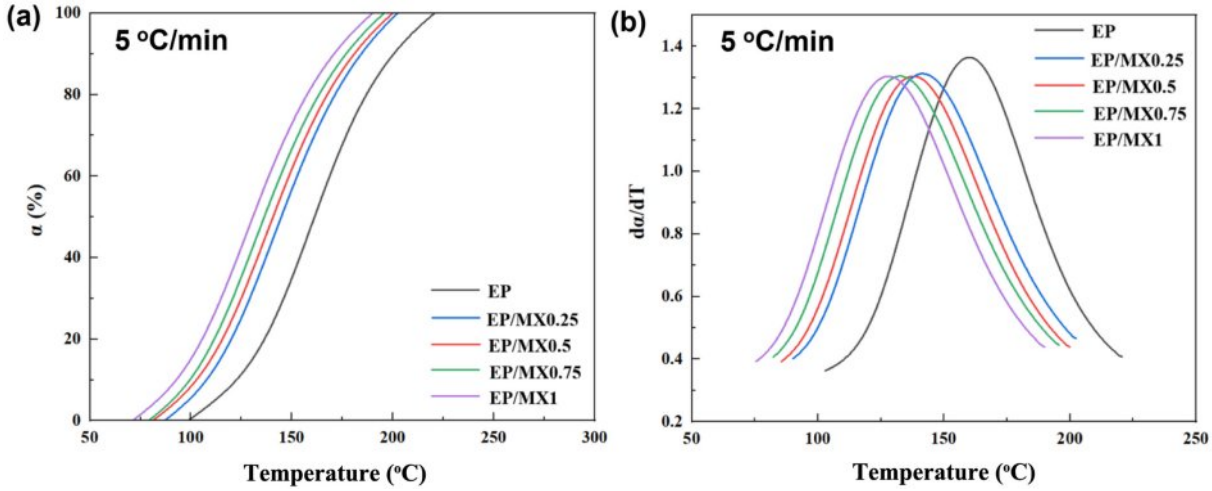

Figure 7. (a) *T*-*α* diagram; (b) T-d*α*/d*T* diagram of EP, EP/MX0.25, EP/MX0.5, EP/MX0.75 and EP/MX1 at the heating rate of 5 ℃/min.

curing stage, as crosslinking reaction progresses, the viscosity gradually becomes larger, and the curing speed becomes slow gradually.

Calculation of Curing Activation Energy. In order to investigate the catalytic behavior of MXenes during EP curing, the Kissinger method was applied to calculate and compare the activation energy of curing reaction E_a of neat EP and EP/MX composite materials.[20,23,33] The Kissinger method formula is shown below:

$$\ln\left(\frac{\beta}{T_p^2}\right) = \ln\left(\frac{A \times R}{E_a}\right) - \frac{E_a}{R} \times \frac{1}{T_p} \quad (1)$$

The activation energy E_a can be calculated based on the slope of $\ln(\beta/T_p^2)$-$1/T_p$. Figure 8 shows the fitted lines obtained based on this, and Table 2 shows the curing activation energy E_a of pure EP and EP/MX composites calculated using the Kissinger method. From Table 2, it can be seen that after adding various concentrations of MXenes, the E_a of EP will decrease. Among them, the E_a of EP/MX1 decreased from 52687 J/mol of pure EP to 40503 J/mol, a decrease of about 20%, indicating that the addition of MXenes has a significant promoting effect on EP curing. Moreover, after adding only 0.5 wt% MXenes, the E_a of EP/MX0.5 is found to be 45234 J/mol, indicating that EP/MX0.5 is very efficient in accelerating the curing of EP.

It is known that for EP, its curing reaction mechanism of is quite complex, and throughout entire curing process, the curing

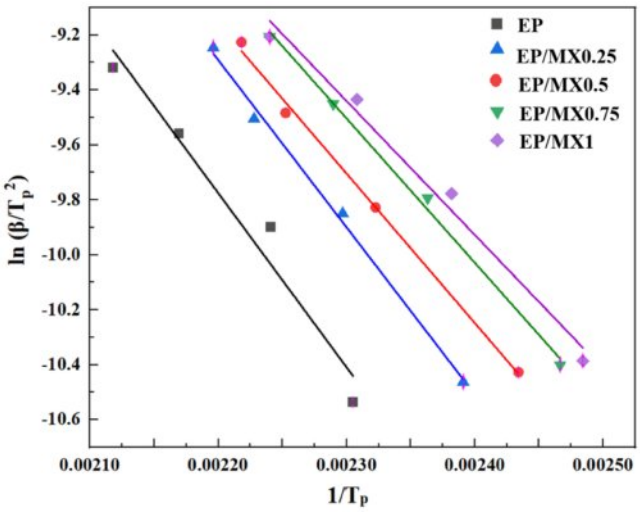

Figure 8. Kissinger plots of $\ln(\beta/T_p^2)$ versus $1/T_p$ of EP, EP/MX0.25, EP/MX0.5, EP/MX0.75 and EP/MX1.

reaction activation energy E_a may change significantly as the reaction progresses. By exploring the changes in E_a, the main controlling factors at different stages of the curing reaction can be identified, which can provide a deeper understanding of the curing mechanism of the EP system and provide theoretical guidance for the study of curing kinetics. The Ozawa method can be used to calculate E_a at different conversion degree α:[21,23,45]

$$\frac{d[\ln(\beta)]}{d[\ln(1/T_p)]} = -1.052\frac{E_a}{R} \quad (2)$$

Table 2. E_a of EP, EP/MX0.25, EP/MX0.5, EP/MX0.75 and EP/MX1

Sample Name	EP	EP/MX0.25	EP/MX0.5	EP/MX0.75	EP/MX1
E_a (J/mol)	52687	50597	45234	42667	40503

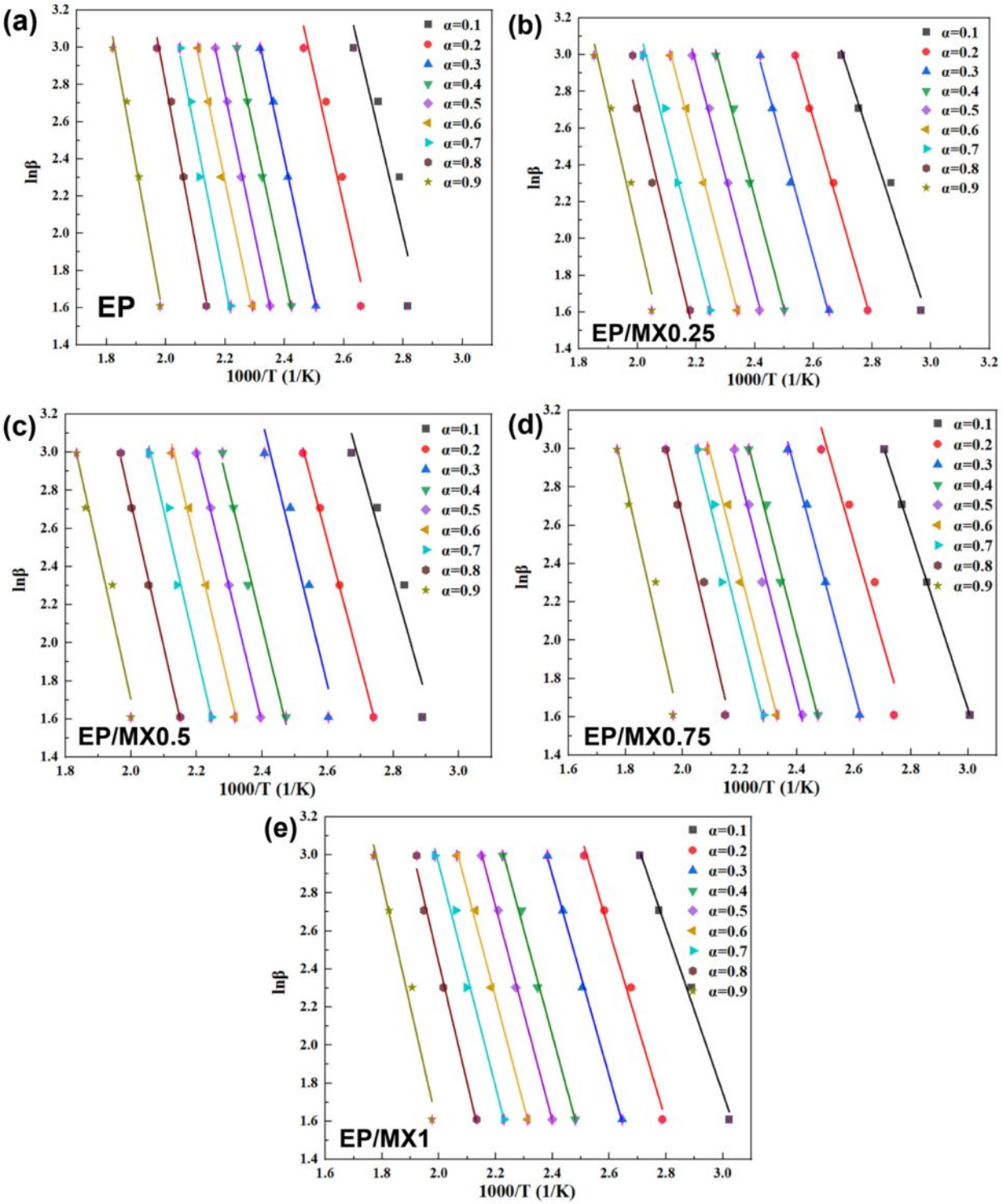

Figure 9. Fitting plots of lnβ versus 1000/T of EP, EP/MX0.25, EP/MX0.5, EP/MX0.75 and EP/MX1.

At the heating rates of 5 ℃/min, 10 ℃/min, 15 ℃/min, and 20 ℃/min, when the conversion degrees are 10, 20, 30, 40, 50, 60, 70, 80, and 90%, the lnβ-1000/T curves of EP, EP/MX0.25, EP/MX0.5, EP/MX0.75, and EP/MX1 can be seen in Figure 9. From the slopes of each fitted line in Figure 9, E_a at different conversion degrees are therefore calculated, as can be seen

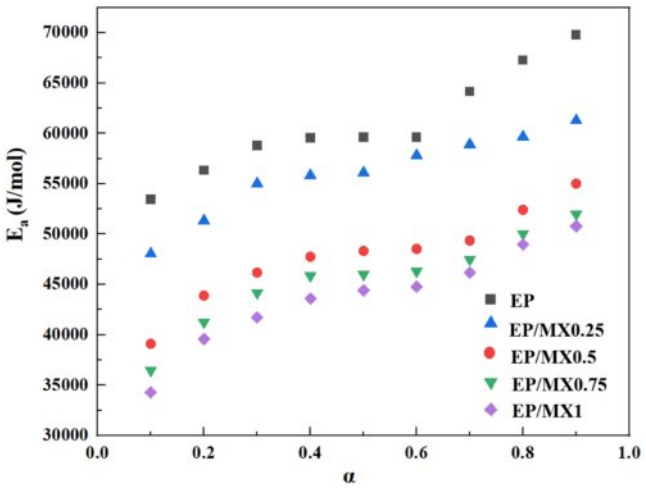

Figure 10. Changes in E_a of EP, EP/MX0.25, EP/MX0.5, EP/MX0.75 and EP/MX1 curing as a function of conversion degree α.

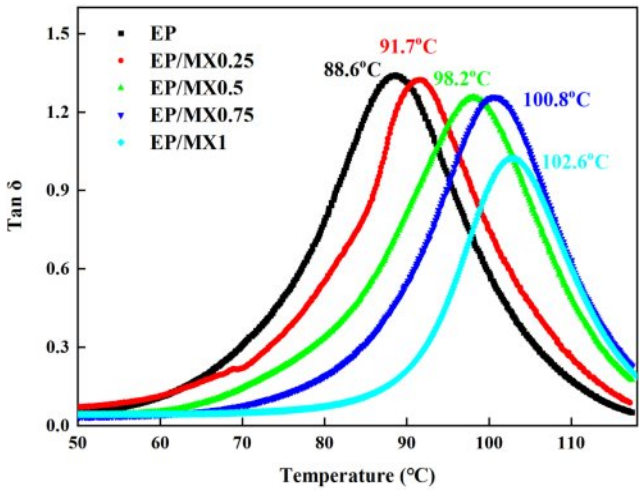

Figure 11. Variation of tanδ as a function of temperature of EP and EP/MXenes composites measured by DMA.

from Figure 10.

From Figure 10, the apparent E_a of EP increases with the increase of conversion degree. This is because: at the beginning stage of curing process, the curing process mainly takes place in the form of chemical reactions between each components. Both EP and EP/MXenes have plenty of reactive groups, which makes chemical reactions occur easily with lower apparent E_a. However, as the curing chemical reaction progresses, the viscosity of the mixture gradually increases, and reactive groups are consumed gradually at the same time. This leads to the solidification reaction gradually being determined by the viscosity of the system, *i.e.*, the diffusion rate of molecules in the system. With the increase of viscosity, the difficulty of reaction molecule movement is enhanced, resulting in a gradual increase in apparent E_a.

At the same conversion degree, regardless of the concentration of MXenes added, the apparent E_a of EP will decrease. The higher the concentration of MXenes, the higher the degree of decrease in apparent E_a. However, overall, when the amount of MXenes added reaches 0.5 wt%, the decrease in apparent E_a is already quite significant. Further increasing the concentration of MXenes resulted in a lower decrease in apparent E_a.

To obtain further understanding, T_g values of the samples were measured by DMA, the obtained tanδ curves of the samples were shown in Figure 11. The T_g values were marked in the figure as well. It can be seen that after adding MXenes, the T_g value of the samples increases gradually with the increase of the MXenes content, which might indicate that the presence of MXenes promotes the crosslinking of EP.

Conclusions

In this study, MXenes ($Ti_3C_2T_x$) were prepared using selective etching method. Its structure was carefully characterized by means of WAXD, SEM and TEM. Results revealed the successful synthesis of MXenes. After that, EP/MXenes composites containing 0.25-1 wt% MXenes were successfully prepared. SEM results of the fractured surface of the samples revealed that the MXenes are finely dispersed in the EP matrix. The curing behavior and related mechanism of EP/MXenes composites were carefully investigated. Results revealed that the addition of MXenes can effectively reduce the curing characteristic temperatures of EP, promoting the curing process to proceed at lower temperatures. Among them, the curing temperatures of EP/MX0.5 with the addition of 0.5 wt% MXenes have significantly decreased, and the curing rate of EP/MX1 with the addition of 1 wt% MXenes is the fastest and reaches the peak curing rate. Moreover, the curing degree of EP/MX1 is the highest; The Kissinger model results showed that the presence of MXenes significantly reduced the activation energy of EP curing reaction (E_a). Within this study, the amount of MXenes added is directly proportional to the degree of reduction in E_a. Compared to pure EP, 52687 J/mol decreased to 40503 J/mol, a decrease of 23.8%; The Ozawa method calculation results show that under the same degree of conversion, the apparent E_a of EP/MX1 is the lowest, but the addition of MXenes does not significantly change the curing behavior of EP. Moreover, results of DMA revealed that the glass transition temperature increases gradually with the increase of the MXenes content, indicating that the presence of

MXenes promotes the crosslinking of EP. The influence of MXenes on the curing behavior of EP was discussed, related mechanism was proposed.

Conflict of interest: The authors declared no potential conflict of interest with respect to the research, authorship, and/or publication of this article.

References

1. Yang, Y.; Wang, D.; Jian, R.; Liu, Z.; Huang, G. Chemical Structure Construction of DOPO-containing Compounds for Flame Retardancy of Epoxy Resin: A Review. *Prog. Org. Coat.* **2023**, 175, 107316.
2. Zhi, M.; Yang, X.; Fan, R.; Yue, S.; Zheng, L.; Liu, Q.; He, Y. A Comprehensive Review of Reactive Flame-retardant Epoxy Resin: Fundamentals, Recent Developments, and Perspectives. *Polym. Degrad. Stabil.* **2022**, 201, 109976.
3. Shundo, A.; Yamamoto, S.; Tanaka, K. Network Formation and Physical Properties of Epoxy Resins for Future Practical Applications. *JACS Au*, **2022**, 2, 1522-1542.
4. Mi, X.; Liang, N.; Xu, H.; Wu, J.; Jiang, Y.; Nie, B.; Zhang, D. Toughness and Its Mechanisms in Epoxy Resins. *Prog. Mater. Sci.* **2022**, 130, 100977.
5. Zhao, Q.; Lu, Z.; Wu, Y.; Zhao, W. Designing Strong Interfacial Adhesion Between Carbon Fiber and Epoxy Resin Via Dopamine Towards Excellent Protection Ability Under High Hydrostatic Pressure and Severe Erosion Corrosion Condition. *Compos. Sci. Technol.* **2022**, 217, 109090.
6. Xue, Y.; Shen, M.; Zeng, S.; Zhang, W.; Hao, L.; Yang, L.; Song, P. A Novel Strategy for Enhancing the Flame Resistance, Dynamic Mechanical and the Thermal Degradation Properties of Epoxy Nanocomposites. *Mater. Res. Express*, **2019**, 6, 125003.
7. An, J.; Zhang,Y.; Zhang, X.; He, M.; Zhou, J.; Zhou, J.; Liu, Y.; Chen, X.; Hu, Y.; Song, X.; Chen, J.; Wu, T.; Kang, J.; Xie, Z. Structure and Properties of Epoxy Resin/Graphene Oxide Composites Prepared from Silicon Dioxide-Modifed Graphene Oxide. *ACS Omega*, **2024**, 9, 17577-17591.
8. Mousavi, S.; Estaji, S.; Kiaei, H.; Mansourian-Tabaei, M.; Nouranian, S.; Jafari, S.; Ruckdäschel, H.; Arjmand, M.; Khonakdar, H. A Review of Electrical and Thermal Conductivities of Epoxy Resin Systems Reinforced with Carbon Nanotubes and Graphene-based Nanoparticles. *Polym. Test.* **2022**, 112, 107645.
9. Liang, X.; Li, X.; Tang, Y.; Zhang, X.; Wei, W.; Liu, X. Hyperbranched Epoxy Resin-grafted Graphene Oxide for Efficient and All-purpose Epoxy Resin Modification. *J Colloid Interf. Sci.* **2022**, 611, 105-117.
10. Imanaka, M.; Narita, I.; Nakamura, Y.; Hisaka, S.; Yoshida, S.; Hara, K. Effect of Matrix Deformability on the Fracture Properties of Epoxy Resins Modified with Core–shell and Cross-linked Rubber Particles. *J. Appl. Polym. Sci.* **2022**, 139, 52316.
11. Gonçalves, F.; Santos, M.; Cernadas, T.; Alves, P.; Ferreira, P. Influence of Fillers on Epoxy Resins Properties: A Review. *J. Mater. Sci.* **2022**, 57, 15183-15212.
12. Su, W.; Han, X.; Gong, J.; Xi, Z.; Zhang, J.; Wang, Q.; Xie, H. Toughening Epoxy Asphalt Binder Using Core-shell Rubber Nanoparticles. *Constr. Build. Mater.* **2020**, 258, 119716.
13. Chen, D.; Gao, F.; Peng, W.; Song, Y.; Hu, R.; Zheng, Z.; Kang, J.; Cao, Y.; Xiang, M. Artificial Water Channels Engineered Thin-film Nanocomposite Membranes for High-efficient Application in Water Treatment. *Sep. Purif. Technol.* **2022**, 303, 122206.
14. Maurya, A.; Sinha, S.; Kumar, P.; Singh, V. A Review: Impact of Surface Treatment of Nanofillers for Improvement in Thermo Mechanical Properties of the Epoxy Based Nanocomposites. *Mater. Today: P.* **2023**, 78, 164-172.
15. Jiang, W.; Liang, Y.; Zhang, Y.; Xie, Z.; Zhou, J.; Kang, J.; Cao, Y.; Xiang, M. Preparation of Graphene Oxide-silica Nanohybrid/poly(Lactic Acid) Biaxially Oriented Films with Enhanced Mechanical Properties. *Polymer* **2022**, 261, 125410.
16. Li, Z.; Gao, H.; Zhang, L.; Liu, J.; Niu, H.; Li, M.; Min, D.; Li, S. Characteristics of Segmental Dynamics in EP/TiO_2 Nanocomposites and Its Effect on Dielectric Breakdown. *Polymer*, **2023**, 270, 125758.
17. An, J.; Chen, Z.; Xie, Z.; Zhou, J.; He, M.; Liu, Y.; Zhang, Y.; Han, L.; Kang, J.; Wu, T.; Chen, J.; Xiang, M. Preparation and Properties of Flexible Dual-network High-performance Epoxy Composites. *Polymer* **2024**, 127621.
18. Wang, L.; Chen, L.; Song, P.; Liang, C.; Lu, Y.; Qiu, H.; Zhang, Y.; Kong, J.; Gu, J. Fabrication on the annealed $Ti_3C_2T_x$ MXene/Epoxy Nanocomposites for Electromagnetic Interference Shielding Application. *Compo. Part B: Eng.* **2019**, 171, 111-118.
19. Kaur, M.; Chawla, H.; Kwatra, N. Effect of GO-modified Epoxy on the Bond Behavior of Old-new Concrete and Comparison with Different Surface Preparation Techniques. *Constr. Build. Mater.*, **2023**, 396, 132369.
20. Yu, Y.; Zeng, F.; Chen, J.;Kang, J.; Yang, F.; Cao, Y.; Xiang, M. Isothermal Crystallization Kinetics and Subsequent Melting Behavior of β-Nucleated Isotactic Polypropylene / Graphene Oxide Composites with Different Ordered Structure, *Polym. Int.* **2018**, 67, 1212-1220.
21. Zhang, F.; Jiang, W.; Song, X.; Kang, J.; Cao, Y.; Xiang, M. Effects of Hyperbranched Polyester-Modified Carbon Nanotubes on the Crystallization Kinetics of Polylactic Acid. *ACS Omega*, **2021**, 6, 10362-10370.
22. Yu, Y.; Zeng, F.; Chen, J.;Kang, J.; Yang, F.; Cao, Y.; Xiang, M. Regulating Polycrystalline Behavior of the β-nucleated Isotactic Polypropylene/graphene Oxide Composites by Melt Memory Effect, *Polym. Compos.* **2019**, 40, E440-E448.
23. Li, L.; Liao, X.; Sheng, X.; Liu, P.; Hao, Z.; He, L.; Qin, G. Influence of Surface Modified Graphene Oxide on the Mechanical Performance and Curing Kinetics of Epoxy Resin. *Polym. Adv. Technol.* **2020**, 31, 1865-1874.
24. Jiang, W.; Sun, C.; Zhang, Y.; Xie, Z.; Zhou, J.; Kang, J.; Cao, Y.; Xiang, M. Preparation of Well-dispersed Graphene Oxide-silica Nanohybrids/poly(lactic acid) Composites by Melt Mixing. *Polym. Test.* **2023**, 118, 107912.

25. Feng, J.; Safaei, B.; Qin, Z.; Chu, F. Effects of Graphene Surface Morphology on Damping Properties of Epoxy Composites. *Polymer* **2023**, 281, 126107.
26. Bazrgari, D.; Moztarzadeh, F.; Sabbagh-Alvani, A.; Rasoulianboroujeni, M.; Tahriri, M.; Tayebi, L. Mechanical Properties and Tribological Performance of Epoxy/Al_2O_3 Nanocomposite. *Ceram. Int.* **2018**, 44, 1220-1224.
27. Zhang, H.; Zhou, H.; Liu, G.; Ge, J.; Jin, L. Mechanical, Dielectric, and Dynamic Mechanical Properties of Al_2O_3–ATP/EP Composites. *J. Mater. Sci.: Mater. Electro.* **2021**, 32, 27871-27881.
28. Zhao, G.; Wang, H.; Ren, J.; Chen, S.; Gao, G.; Wang, N.; Yang, Y. The Tribological Behaviors of Core-shell *n*-octadecane@TiO_2/epoxy Composites. *Polym. Compos.* **2020**, 41, 4872-4884.
29. Hanhai Dong, Yixuan Qiao, Song Peng, Yuqi Li, Yongqian Zhen, Wei Tan, Qingli Cheng, Yang Wang, 2D Material/epoxy Composite Coatings, a Perspective from the Regulation of 2D Materials. *Progress in Organic Coatings*, **2023**, 183, 107817.
30. Sensen Han, Qingshi Meng, Zhe Qiu, Amr Osman, Rui Cai, Yin Yu, Tianqing Liu, Sherif Araby, Mechanical, Toughness and Thermal Properties of 2D Material-reinforced Epoxy Composites, *Polymer* **2019**, 184, 121884.
31. Peng, W.; Kang, J.; Song, X.; Zhang, Y.; Hu, B.; Cao, Y.; Xiang, M. Investigation on the Effects of MXene and *β*-Nucleating Agent on the Crystallization Behavior of Isotactic Polypropylene. *Polymers* **2021**, 13, 2931.
32. Giménez, R.; Serrano, B.; San-Miguel, V.; Cabanelas, J. Recent Advances in MXene/Epoxy Composites: Trends and Prospects. *Polymers* **2022**, 14, 1170.
33. Jiang, W.; Chen, D.; Xie, Z.; Zhang, Y.; Hu, B.; Kang, J.; Cao, Y.; Xiang, M. Exploring the Size Effect of Graphene Oxide on Crystallization Kinetics and Barrier Properties of Poly(lactic acid). *ACS Omega* **2022**, 7, 37315-37327.
34. Chen, D.; Hu, R.; Song, Y.; Gao, F.; Peng, W.; Zhang, Y.; Xie, Z.; Kang, J.; Zheng, Z.; Cao, Y.; Xiang, M. Hydrophilic Modified Polydopamine Tailored Heterogeneous Polyamide in Thin-film Nanocomposite Membranes for Enhanced Separation Performance and Anti-fouling Properties. *J. Membrane Sci.* **2023**, 666, 121124.
35. Anasori, B.; Lukatskaya, M.; Gogotsi, Y. 2D Metal Carbides and Nitrides (MXenes) for Energy Storage. *Nat. Rev. Mater.* **2017**, 2, 16098.
36. Xu, R.; Gao, F.; Wu, Y.; Ding, L.; Chen, D.; Liu, T.; Yu, Y.; Zhuo, W.; Chen, Z.; Zhang, Y.; Sun, Y.; Yang, F.; Chen, J.; Cao, Y.; Kang, J.; Zheng, Z.; Xiang, M. Influences of Support Layer Hydrophilicity on Morphology and Performances of Polyamide Thin-film Composite Membrane. *Sep. Purif. Technol.* **2022**, 281, 119884.
37. Xiong, B.; Chen, R.; Zeng, F.; Kang, J.; Men, Y. Thermal Shrinkage and Microscopic Shutdown Mechanism of Polypropylene Separator for Lithium-ion Battery: In-situ Ultra-small Angle X-ray Scattering Study. *J. Membrane Sci.* **2018**, 545, 213-220.
38. Wang, J.; Xu, R.; Yang, F.; Kang, J.; Cao, Y.; Xiang, M. Probing Influences of Support Layer on the Morphology of Polyamide Selective Layer of Thin Film Composite Membrane. *J. Membrane Sci.* **2018**, 556, 374-383.
39. Liu, T.; Chen, D.; Cao, Y.; Yang, F.; Chen, J.; Kang, J.; Xu, R.; Xiang, M. Construction of a Composite Microporous Polyethylene Membrane with Enhanced Fouling Resistance for Water Treatment. *J. Membrane Sci.* **2021**, 618, 118679.
40. Shen, B.; Hu, Y.; Song, X.; Song, Z.; Liu, J.; Sun, C.; Lu, S.; Kang, J.; Cao, Y.; Xiang, M.; Zheng, Z. Study on the Evolution Mechanism of the Structure and Properties of ABS in Cycled Fused Deposition Molding (FDM). *Ind. Eng. Chem. Res.* **2023**, 62, 13572-13580.
41. Xu, R.; Wang, J.; Chen, D.; Liu, T.; Zheng, Z.; Yang, F.; Chen, J.; Kang, J.; Cao, Y.; Xiang, M. Preparation and Performance of a Charge-mosaic Nanofiltration Membrane With Novel Salt Concentration Sensitivity for the Separation of Salts and Dyes. *J. Membrane Sci.* **2020**, 595, 117472.
42. Kang, J.; Chen, D.; Xiong, B.; Zheng, N.; Yang, F.; Xiang, M.; Zheng, Z. A Facile Route for the Fabrication of Polypropylene Separators for Lithium Ion Batteries with High Elongation and Strong Puncture Resistance. *Ind. Eng. Chem. Res.* **2019**, 58, 23135-23142.
43. Yu, Y.; Xiong, B.; Zeng, F.; Xu, R.; Yang, F.; Kang, J.; Xiang, M.; Li, L.; Sheng, X.; Hao, Z. Influences of Compression on the Mechanical Behavior and Electrochemical Performances of Separators for Lithium Ion Batteries. *Ind. Eng. Chem. Res.* **2018**, 57, 17142-17151.
44. Zeng, F.; Xu, R.; Ye, L.; Xiong, B.; Kang, J.; Xiang, M.; Li, L.; Sheng, X.; Hao, Z. Effects of Heat Setting on the Morphology and Performances of Polypropylene Separator for Lithium Ion Batteries. *Ind. Eng. Chem. Res.* **2019**, 58, 2217-2224.
45. Yu, Y.; Zeng, F.; Chen, J.; Kang, J.; Yang, F.; Cao, Y.; Xiang, M. Effects of Ordered Structure on Non-isothermal Crystallization Kinetics and Subsequent Melting Behavior of *β*-nucleated Isotactic Polypropylene/graphene Oxide Composites. *J. Therm. Anal. Calorim.* **2019**, 136, 1667-1678.
46. Chen, D.; Liang, Q.; Gao, F.; Liu, T.; Wu, Y.; Zheng, Z.; Kang, J.; Xu, R.; Cao, Y.; Xiang, M. Design of High-performance Biomimetic Reverse Osmosis Membranes by Introducing Loose Liposome as An Artificial Water Channel. *Chem. Eng. J.* **2022**, 431, 133878.
47. Gao, F.; Liu, H.; Zhang, Y.; Liu, D.; Xie, Z.; Peng, W.; Song, Y.; Hu, R.; Chen, D.; Kang, J.; Xu, R.; Cao, Y.; Xiang, M. Polyamide Membrane with Nanoscale Stripes and Internal Voids for High-performance Nanofiltration. *J. Membrane Sci.* **2023**, 671, 121406.